Science Bulletin xxx (xxxx) xxx

Contents lists available at ScienceDirect

Science Bulletin

journal homepage: www.elsevier.com/locate/scib

Article

Piezocatalytically-induced controllable mineralization scaffold with bone-like microenvironment to achieve endogenous bone regeneration

Xi Cui [a,b,1], Lingling Xu [c,1], Yizhu Shan [a,b], Jiaxuan Li [a,b], Jianying Ji [a], Engui Wang [a], Baokun Zhang [a], Xiaozhou Wen [a,b], Yuan Bai [a], Dan Luo [a,b,*], Chunying Chen [c,*], Zhou Li [a,b,*]

[a] Beijing Key Laboratory of Micro-nano Energy and Sensor, Beijing Institute of Nanoenergy and Nanosystems, Chinese Academy of Sciences, Beijing 101400, China
[b] School of Nanoscience and Engineering, University of Chinese Academy of Sciences, Beijing 100049, China
[c] New Cornerstone Science Laboratory, CAS Key Laboratory for Biomedical Effects of Nanomaterials and Nanosafety and CAS Center for Excellence in Nanoscience, National Center for Nanoscience and Technology, Beijing 100190, China

ARTICLE INFO

Article history:
Received 27 February 2024
Received in revised form 18 March 2024
Accepted 22 March 2024
Available online xxxx

Keywords:
Piezoelectric catalysis
Controllable mineralization
Biomimetic
Bone repair
Biodegradable

ABSTRACT

Orderly hierarchical structure with balanced mechanical, chemical, and electrical properties is the basis of the natural bone microenvironment. Inspired by nature, we developed a piezocatalytically-induced controlled mineralization strategy using piezoelectric polymer poly-L-lactic acid (PLLA) fibers with ordered micro-nano structures to prepare biomimetic tissue engineering scaffolds with a bone-like microenvironment (pcm-PLLA), in which PLLA-mediated piezoelectric catalysis promoted the *in-situ* polymerization of dopamine and subsequently regulated the controllable growth of hydroxyapatite crystals on the fiber surface. PLLA fibers, as analogs of mineralized collagen fibers, were arranged in an oriented manner, and ultimately formed a bone-like interconnected pore structure; in addition, they also provided bone-like piezoelectric properties. The uniformly sized HA nanocrystals formed by controlled mineralization provided a bone-like mechanical strength and chemical environment. The pcm-PLLA scaffold could rapidly recruit endogenous stem cells, and promote their osteogenic differentiation by activating cell membrane calcium channels and PI3K signaling pathways through ultrasound-responsive piezoelectric signals. In addition, the scaffold also provided a suitable microenvironment to promote macrophage M2 polarization and angiogenesis, thereby enhancing bone regeneration in skull defects of rats. The proposed piezocatalytically-induced controllable mineralization strategy provides a new idea for the development of tissue engineering scaffolds that can be implemented for multimodal physical stimulation therapy.

1. Introduction

Bone defects are a common clinical condition in patients with severe infections, osteoporosis, or those who have suffered from traffic accidents, tumor resection, and sports injuries [1,2]. Although bone tissue has self-healing ability after injury, large-area bone damages exceeding a critical size still require surgical implantation of bone grafts to restore bone structure and function. Autologous bone and allogeneic bone are ideal bone repair materials, but their limited sources, high risk of infection, susceptibility to immune rejection, and difficulty in processing limit their application in clinical practice [3,4]. In order to develop ideal alternatives for autograft bone, extensive research has been conducted over the past few decades to fabricate various bone biomimetic scaffolds. To date, materials such as metals, self-assembled biomolecules, polymers, and ceramics have been used to create bone graft scaffolds with morphological and mechanical properties similar to natural bone [5,6]; however, the aforementioned conventional bone implant materials are difficult to reconstitute a multifunctionally balanced bone microenvironment due to their monofunctionality. It is still challenging to prepare biomimetic materials that simulate the osteogenic microenvironment in terms of bone structure, chemical composition, and physicochemical properties [7,8].

The natural bone microenvironment is a hierarchical structure with balanced mechanical, chemical and electrical properties. Biomacromolecule collagen and inorganic hydroxyapatite (HA) self-assemble to form a hierarchical structure, in which inorganic calcium and phosphorus nanocrystals with controllable and regular dimensions are attached to the internal and external spaces of

* Corresponding authors.
E-mail addresses: luodan@binn.cas.cn (D. Luo), chenchy@nanoctr.cn (C. Chen), zli@binn.cas.cn (Z. Li).
[1] These authors contributed equally to this work.

https://doi.org/10.1016/j.scib.2024.04.002
2095-9273/

the assembled collagen fibers [9]. This controlled mineralization structure not only gives the bone sufficient mechanical strength but also serves as a storage reservoir for calcium phosphate, which can be slowly degraded into Ca^{2+} and PO_4^{3-} locally to regulate the chemical microenvironment for bone regeneration [10]; more importantly, the asymmetric molecular structure of collagen fibers endows bone with unique piezoelectric properties [11]. A balanced mechanical, chemical, and electrical microenvironment plays a crucial role in bone growth and development. Specifically, the ordered assembly interface of mineralized fibers is beneficial to cell adhesion, migration, and angiogenesis [12,13]; the improvement of mechanical properties caused by mineralization can promote the osteogenic differentiation of stem cells through piezo family; the sustained release of Ca^{2+} and PO_4^{3-} ions creates a chemotactic environment for osteoblasts, which promote osteogenic differentiation by upregulating bone morphogenetic protein 2 (BMP2) expression [14,15]; piezoelectric properties of natural bone have been shown to regulate osteogenic differentiation through activation of cell membrane calcium channels [16–18], surface receptor redistribution and signaling pathways such as mitogen-activated protein kinases (MAPK) [16,17] and phosphatidylinositol 3-kinase (PI3K) [19]. In summary, simulating the bone-like microenvironment by reconstructing an orderly mineralized interface and achieving a balance of mechanical, chemical, and electrical properties is the key to effectively regulating endogenous bone regeneration.

Constructing scaffold materials with a three-dimensional (3D) hierarchical structure and providing effective mechanical support has been extensively studied [20,21]; however, endowing bioactive scaffolds with a bone-like electrical microenvironment remains a challenge. Piezoelectric materials do not rely on a connected power source and can produce electrical output through only non-invasive stimulation with ultrasound (US), making them ideal materials for simulating electrical microenvironments [22,23]. Although piezoelectric ceramics and piezoelectric polymers have been shown to promote osteogenic differentiation of stem cells, interestingly, just as it is difficult to impart electrical properties to mineralized scaffolds, piezoelectric materials are also difficult to integrate appropriate chemical and mechanical properties [5,24,25]. Currently, the use of piezoelectric materials to construct bone microenvironments with balanced mechanical, chemical, and electrical properties faces the following three challenges: (1) Uncontrolled mineralization: whether it is electrospinning technology for fabricating piezoelectric polymers or mixing, doping or self-assembly strategies for processing nanoceramics, doping calcium-phosphorus crystals face the problem of uncontrollable crystal nucleation and growth, which leads to the formation of micrometer-scale or even larger mineralized crystals and covering the surfaces of piezoelectric materials, deactivating their electroactivities [26,27]. (2) Mismatch in mechanical properties: ceramics are hard but also brittle, making them difficult to process. More importantly, long-term implantation of materials with high mechanical strength will damage the surrounding bone tissue, resulting in a reduction in bone density [28–30]. In comparison, piezoelectric polymers, while easy to process, cannot provide adequate mechanical support. (3) Lack of biodegradability: most piezoelectric materials are non-biodegradable, and undegraded residues can seriously affect bone remodeling [8,31]. This dilemma highlights the urgency of developing new piezoelectric-based materials for bone tissue engineering to enable effective integration of traditional mineralized bone grafting materials with innovative electrical stimulation therapy concepts.

An ideal piezoelectric scaffold that can simulate the bone microenvironment should have the following characteristics: (1) Exhibiting an ordered interface structure with balanced mechanical, chemical, and electrical properties; (2) presenting sufficient mechanical support strength without causing damage to surrounding tissues; (3) possessing a degradation rate compatible with the rate of tissue remodeling. In this work, we proposed a piezocatalytically-induced controllable mineralization strategy based on the degradable piezoelectric polymer poly-L-lactic acid (PLLA) [32,33], and constructed a tissue engineering scaffold (pcm-PLLA) that simulates the bone-like microenvironment in terms of morphological structure, mechanical, chemical, and electrical properties (Fig. 1a). After applying ultrasonic stimulation, the piezoelectric catalytic reaction occurring on the surface of oriented PLLA promoted the polymerization of dopamine (DA) [23,34,35] and subsequently regulated the growth of HA crystals, ultimately obtaining a tissue engineering scaffold with a surface mineralization layer and retaining electrical activity. The piezocatalytically-induced controllable mineralization strategy endowed piezoelectric fibers with bone-like mechanical properties. In addition, the catalytically formed HA nanocrystals were uniformly deposited on the fiber surface with a suitable scale, and continuously released Ca^{2+} and PO_4^{3-} during the degradation process, creating a suitable chemical microenvironment for bone growth. More importantly, the piezoelectric signal from PLLA was not shielded by the controllable mineralization layer. The *in vitro* experiments demonstrated that endogenous stem cells were rapidly recruited into the interconnected pore structure of the scaffold, achieving quick integration of the scaffold and bone [36,37]. The electrical signal output induced by ultrasound can stimulate the differentiation of stem cells into osteoblasts, thus promoting the bone regeneration process. In the rat skull defect model, the appropriate microenvironment provided by the scaffold not only upregulated macrophage M2 type polarization, but also rapidly initiated angiogenesis (Fig. 1b). Only 4 weeks after implantation, 87.9%±1.6% of the defect area in the pcm-PLLA group was filled with new osteogenic tissue. Importantly, the scaffold was able to be completely degraded and absorbed by the organism after inducing endogenous bone regeneration (Fig. 1c). The mRNA transcriptome sequencing further revealed the mechanism by which pcm-PLLA promoted bone repair by upregulating the PI3K signaling pathway. The piezocatalytically-induced controlled mineralization strategies provide new ideas for the development of multimodal physical stimulation scaffolds for hard tissue regeneration.

2. Materials and methods

2.1. Fabrication of PLLA piezoelectric scaffolds

Pcm-PLLA scaffold fabrication consists of three steps. Firstly, PLLA with a molecular weight of 300,000 was dissolved in hexafluoroisopropanol (aladdin) at a concentration of 10% for 2 h of stirring. Specifically, a 5 mL syringe with a 23-gauge needle was placed 10 cm from the receiver working at a flow rate of 1 mL/h, the positive high voltage was set to 10 kV, the negative high voltage was set to −3 kV, the speed of the receiver was 1800 r/min, and the total time of work was 90 min. The PLLA fiber membranes obtained by electrostatic spinning were placed in a vacuum oven overnight to fully evaporate the residual organic solvents, and then were subjected to high temperature treatment at 120 °C for 4 h. Secondly, dopamine hydrochloride solution at a concentration of 2 mg/mL was prepared in Tris solution at pH 8.4, and the PLLA membrane was submerged in the solution and worked under ultrasound in a water bath for 1 h to obtain the polydopamine (PDA) coating. Finally, an aqueous HA solution of 5 mg/mL was prepared and dispersed under ultrasound for 10 min, and then the PDA/PLLA obtained in the previous step was submerged in the solution and continued to ultrasound for 1 h (or 0.5, 2 h) to

Please cite this article as: X. Cui, L. Xu, Y. Shan et al., Piezocatalytically-induced controllable mineralization scaffold with bone-like microenvironment to achieve endogenous bone regeneration, Science Bulletin, https://doi.org/10.1016/j.scib.2024.04.002

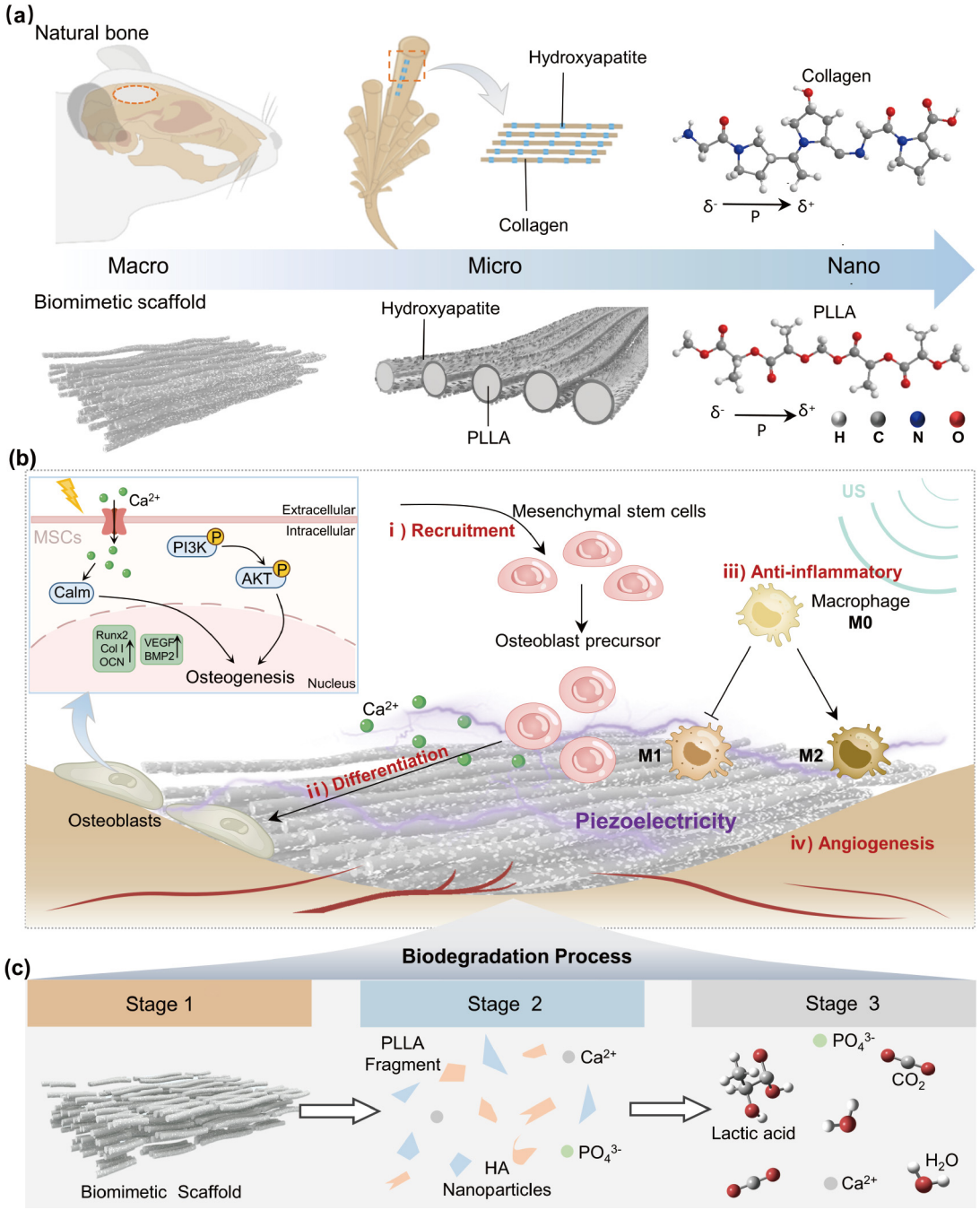

Fig. 1. Formation of a bionic piezoelectric bone scaffold and its biological effects. (a) Biomimetic scaffolds from macro, micro to nano mimic the structural, mechanical, electrical, and chemical properties of natural bone. Natural bone consists of an ordered structure of piezoelectric collagen fibers and HA arranged with collagen fibers, the corresponding biomimetic scaffolds consist of ordered piezoelectric PLLA fibers and HA particles on the surface. (b) Piezoelectric bionic scaffolds act on bone defects in four ways: stem cell recruitment, stem cell differentiation, anti-inflammatory, and angiogenesis, and lead to bone regeneration. Scaffold releases calcium ions to alter chemical environment, allowing recruitment of stem cells, which are differentiated towards osteogenesis by ultrasound piezoelectricity. The bone-like microenvironment promotes M2-type polarization of macrophages and increased angiogenesis. Scaffolds promote osteogenic differentiation by affecting calcium channels in MSCs and the PI3K signaling pathway. (c) The biodegradation process of the scaffold can be divided into three stages: stage 1, the long fibers are explained into short fibers; stage 2, the short fibers are degraded into PLLA fragments, the HA nanoparticles are degraded into small particles and release Ca^{2+} as well as PO_4^{3-}; stage 3, all of the PLLA is degraded into lactic acid, water and carbon dioxide.

obtain HA/PDA/PLLA scaffold (pcm-PLLA). The scaffolds were rinsed under running water and dried for subsequent experiments.

2.2. Characterization of scaffold

The microstructure and elemental composition of the nanofibers was characterized by Nova 450 scanning electron microscope (SEM) and Raith/EDAX energy dispersive spectrometer (EDS). Nano Measure software was then used to evaluate the size distribution of the PLLA nanofibers. The hydrophilicity of the nanofibers was evaluated using a contact angle measuring instrument (OCA25; Data physics corporation, Germany). X-ray diffraction (XRD) was performed with a PANalytical X'Pert3 diffractometer (PANalytical Ltd., Netherlands) loaded a Cu Kα source with a step of 0.013°

and a 2θ range from 5° to 80°. Fourier transform infrared spectrometer spectra were obtained using Vertex 80 V (Bruker Corp, MA, USA), and Raman spectra were obtained using LabRAM HR Evolution. Transmission electron microscopic (TEM) photographs were obtained on a Tecnai G2 20 TWIN UEM. X-ray photoelectron spectroscopy (XPS) spectrum was conducted on an ESCAlab250 (Thermal Scientific, USA). Piezoresponse force microscopic (PFM) measurements were characterized by an atomic force microscope (AFM) (NTEGRA, MFP-3D-SA) equipped with a ferroelectric test system. Microscopic Young's modulus was tested by Bruker Dimension ICON.

2.3. Measurement of open-circuit output voltage under ultrasound

A layer of metallic silver was magnetron sputtered as an electrode on both sides of a 1 cm × 1 cm thin film support, which was prepared by magnetron sputtering (PVD75 Kurt J. Lesker, Ar, 4 mTorr, 100 W, 15 min). To avoid frictional electrical signals from interfering with its output, the film was sealed with polytetrafluoroethylene (PTFE) tape, and both sides of the film were connected to the positive and negative terminals of the oscilloscope (HDO 6104) via copper leads. The film was immersed in silicone oil to shield it from external interference, ultrasound was applied to the film at 1 W/cm^2, 1 MHz with an ultrasound probe to drive the piezoelectricity, and the piezoelectric voltage output of the film was recorded with an oscilloscope.

2.4. Determination of d_{14} piezoelectric coefficient

We tested the d_{14} piezoelectric coefficient of the films using a laboratory-built d_{14} piezoelectric coefficient testing rig. Specifically, a force of a specific magnitude was applied to the film parallel to the fiber direction, and then the piezoelectric signals generated on both sides of the film were captured, and the d_{14} piezoelectric coefficient of the film was calculated using the following equation:

$$d_{14} = \frac{D_{sur}}{T_4} = \frac{Q_{sur}}{A_{sur}} \left(\frac{F}{A_{cro}} \right)^{-1} = \frac{A_{cro}}{A_{sur}} \hat{A} \cdot \frac{\int I dt}{F}, \quad (1)$$

where D_{sur} is the surface charge density, T_4 is the applied stress along the shear direction, Q_{sur} is the generated surface charge, A_{sur} is the surface area, F is the applied force, A_{cro} is the cross-sectional area, I is the current, and t is the time.

2.5. Obtaining and culture primary mesenchymal stem cells (MSCs)

MSCs were extracted from the skull of 3-day-old SD rats according to surgical protocol. Specifically, the rats were decapitated and their skin was sterilized with alcohol, and then the skull was carefully peeled off and digested with trypsin at 37 °C for 10 min. Trypsin was discarded and replaced with 1 mg/mL of collagenase I for 30 min at 37 °C. Bones were then cut into small pieces and replaced with fresh collagenase I for 1 h, after which the supernatant was centrifuged to obtain the MSCs. MSCs were passaged to generation 3–6 for subsequent experiments using α-MEM medium (Gibco). MSCs were cultured in α-MEM medium (Gibco) supplemented with 10% fetal bovine serum (Gibco), 1% penicillin streptomycin (Solarbio). Osteogenic differentiation medium was supplemented with 0.01 mmol/L dexamethasone (Dex), 10 mmol/L sodium β-glycerophosphate, and 0.5 mmol/L ascorbic acid. The incubator was set at 37 °C with 5% CO_2 environment and the cell culture medium was changed every 2–3 days.

2.6. Cell morphology and cytoskeleton detection

All samples were fixed in 4% paraformaldehyde for 10 min at room temperature and then soaked in permeabilization buffer for 5 min at 4 °C. The samples were washed with phosphate buffer saline (PBS) buffer and then incubated with Rhodamine-Phalloidin (Abcam, 1:1000) for 1 h at 37 °C. The samples were washed with PBS buffer and incubated with 4′,6-diamidino-2 phenylindole (DAPI, Invitrogen, Beijing Solarbio Science & Technology Co., Ltd., 1:200) at 37 °C for 10 min, then washed with PBS. The samples were covered with glass coverslips for observation with a laser confocal microscope (TCS SP8, Leica).

2.7. Immunostaining

All samples were fixed in 4% paraformaldehyde for 10 min at room temperature and then rinsed with PBS buffer. The samples were then incubated with 10% goat serum at 37 °C for 30 min and the goat serum was washed off with PBS buffer. The prepared primary antibody was added and left overnight at 4 °C, which was washed with PBS and the secondary antibody (1:200) was added and kept at 37 °C for 30 min. 10 min of DAPI was added to the samples and the samples were covered with coverslips for the next step of the laser confocal microscope observation.

2.8. Quantitative real-time polymerase chain reaction analysis (qPCR)

RNA was extracted from the cells according to the manufacturer's instructions for RC112-01 (FastPure® Cell/Tissue Total RNA Isolation Kit V2, Vazyme Biotech Co., Ltd.) and its concentration was assayed with a nanodrop. The reverse transcription system was prepared as follows: 1000 ng RNA, 4 μL 5 × RT Master mix, and RNase free water was added to made up to 20 μL. The solution was mixed well and then put into the PCR machine for the reaction under the following conditions: 37 °C, 30 min → 85 °C, 1 min → 4 °C. The cDNA was diluted with ddH_2O to a concentration of 2.5 ng/μL after reverse transcription. Prepare the qPCR reverse transcription system according to the instructions of the reagent R323-01 reagent: 5 μL SYBR, 0.4 μL pre and post primer, 2 μL cDNA, RNase free water made up to 10 μL. The primer sequences are shown in Table S1 (online). The solution system was mixed well and put into the PCR machine for the reaction under the following conditions: 37 °C, 15 min → 85 °C, 5 s. Threshold cycle (Ct) values were obtained by processing using the ΔΔCt method to analyze gene expression.

2.9. Alkaline phosphatase (ALP) activity

Each well of cells was lysed and incubated with 5 μL of ALP reaction liquid for 10 min at 37 °C according to the manufacturer's instructions (Alkaline Phosphatase (AKP/ALP) Activity Assay Kit, Beijing Solarbio Science & Technology Co., Ltd.). Then 100 μL of reaction termination liquid was added to each well, at which point the liquid would take on a different color. The absorbance of the liquid at 510 nm, which is proportional to the amount of ALP, was measured using an enzyme marker.

2.10. Animals and surgical procedures

Female SD rats weighing around 220 g (6–8 weeks) were purchased from Vital River Co (Beijing, China). All animal experiments were approved by the Committee on Ethics of Beijing Institute of Nanoenergy and Nanosystems (2022005LZ). All surgeries were performed in a sterile environment and the surgical instruments involved were autoclaved before surgery. A 5-mm diameter circular bone defect was created on the midline suture of the SD rat by

Please cite this article as: X. Cui, L. Xu, Y. Shan et al., Piezocatalytically-induced controllable mineralization scaffold with bone-like microenvironment to achieve endogenous bone regeneration, Science Bulletin, https://doi.org/10.1016/j.scib.2024.04.002

electric drill, taking great care of the rat's brain during the drilling process. The sterilized scaffold was cut to the shape of the defect, placed into the defect location and then fixed with light-cured hydrogel and irradiated with UV light for 10 s. The wound was sutured and sterilized with iodophor and 0.5 mL of penicillin was injected intraperitoneally into each rat to prevent wound infection. The rats were euthanized after 10 days or 12 weeks and the skulls and vital organs (heart, liver, spleen, lungs, and kidneys) were obtained for further analysis.

2.11. Micro-computed tomography scanning evaluation

At 10 days, 4 weeks and 12 weeks postoperatively, the μ-CT imaging system (Quantum GX) was used to assess new bone formation within the implants of the harvested specimens. During scanning, the specimens were imaged with a spot size of 4.5 μm and a maximum voltage of 70 kV. After reconstruction with a high-resolution protocol, the acquired images were further analyzed using the Radiant software, in which newly formed bone tissue was segmented from each implant using a global threshold. After segmentation, the bone volume fraction was calculated by normalizing the bone volume to the total volume of the implant macropores.

2.12. Histological analysis

In order to evaluate the regeneration of the new bone tissue as well as the health status of the rats, histological staining was performed, which included hematoxylin-eosin staining (H&E), Masson's trichrome (MT) as well as immunofluorescence staining and immunohistochemical staining. No fewer than three rats were used in each group, and each sample was cut into 6-μm paraffin sections for staining. The skulls were fixed in formalin and then decalcified for 50 days before paraffin sectioning.

2.13. Statistical analysis

All semi-quantitative analyses of the images were performed using the image J software. All data are expressed as mean ± standard deviation. One-way analysis of variance method was used to analyze statistically significant differences (P) between different groups. $P < 0.05$ was considered statistically significant.

3. Results

3.1. Preparation and characterization of pcm-PLLA

The piezoelectric PLLA scaffolds with surface-loaded HA were obtained through a three-step process. PLLA fiber film was obtained via electrospinning, demonstrating a high degree of orientation (Fig. S1 online). The fibers were modified layer-by-layer with DA and HA (Fig. S2 online) using sequential ultrasonic piezoelectric catalysis, resulting in a pcm-PLLA scaffold (Fig. 2a). Both scaffolds are flexible, thickness-adjustable films that can be bent, stretched, folded, and twisted (Fig. 2b and Fig. S3 online). In accelerated degradation experiments *in vitro*, partial fracture of pcm-PLLA scaffolds was observed at 2 weeks, and almost completely broken into fragments after 8 weeks (Fig. 2c). As a bridge layer, PDA can form electrostatic forces with PLLA and hydrogen bonds with hydroxyl groups of HA, resulting in a tighter and more uniform loading of HA on the fiber surface. Specifically, PLLA generates a negative charge in response to ultrasound, electrostatically attracting positively charged DA to polymerize on its surface. Furthermore, the HA nanoparticles were dispersed using ultrasound to facilitate their rapid growth on the fiber surface through hydrogen bonding (Fig. 2d). From the SEM images in Fig. S4 (online), the traditional immersion method involves the formation of a membrane on the surface of PLLA fiber scaffolds by PDA, which covers the 3D structure of the scaffolds. Furthermore, additional deposited HA particles have a tendency to agglomerate, which is unfavorable for cell growth. In contrast, the ultrasonic piezoelectric approach enables uniform aggregation of PDA on the fiber surface in a shorter period of time (from 24 h to 30 min). This approach not only preserves the pore structure between the fibers but also allows for controlled mineralization layer thickness by adjusting the HA modification time (Fig. 2e). When the modification time of HA was 60 min, the fibers surface was almost completely covered by HA nanoparticles that were grown *in situ* (Fig. 2e). To examine the interfacial force between HA and PLLA fibers, we simulated the treatment process by performing a prolonged ultrasonic cleaning of the pcm-PLLA2 scaffolds in deionized water. After 30 min of ultrasonic cleaning, the pcm-PLLA scaffold fibers remained coated with a sufficient number of HA nanoparticles, indicating that HA was tightly bound to the fiber surface (Fig. 2f).

Furthermore, a series of characterizations were carried out to demonstrate the successful preparation of pcm-PLLA scaffolds. AFM images further confirmed the orientation and high porosity between the fibers of the pcm-PLLA scaffold (Fig. S5 online). With the modification of PDA and HA, the diameters of the scaffold fibers gradually increased, which were around 500–800 nm (Fig. S6 online). According to the results of the EDS analysis, the Ca/P ratio on the pcm-PLLA scaffolds was 1.71, which is comparable to that in natural bone (Fig. 2g and Fig. S7 online). Furthermore, annealing is a key factor affecting PLLA crystallinity and piezoelectricity. In this study, the unannealed PLLA film was named PLA, and the PLLA film that was annealed at 140 °C for 8 h was named PLLA. XRD test results show that annealing significantly improves the crystallinity of PLLA in α and α' crystal phases (Fig. 2h) [38]. The XRD characteristic peaks of pcm-PLLA corresponded to the standard cardinal peaks of HA (JCPDS No 09-0432), indicating that HA was successfully modified on PLLA. Fourier transform infrared spectrometer, XPS, and Raman spectroscopy results also further confirmed the successful modification of PDA and HA (Fig. S8a–c online). The incorporation of PDA and HA nanoparticles greatly enhanced the hydrophilicity of the scaffold surface (Fig. S8d online).

In order to obtain mechanical strengths more suitable for osteogenic growth, we have explored the Young's modulus of scaffolds using piezoelectric-catalyzed realization of controlled mineralization. The degree of mineralization affects the Young's modulus and piezoelectric output of the scaffold, which have a crucial role in promoting osteogenic differentiation processes. We therefore tested the microscopic Young's modulus and piezoelectric output of scaffolds with different mineralization times (pcm-PLLA1, pcm-PLLA2, pcm-PLLA3 in Fig. 2e). The Young's modulus of scaffolds was calculated from force-displacement curves of AFM, which increased with increasing HA modification (Fig. 2i). Compared with PLLA, the incorporation of HA enhances the Young's modulus of the fibers to 5.4 GPa, which approaches the microscopic Young's modulus of bone [4,28]. The results of the stress–strain curve tests also showed that the modification of HA increased the macroscopic Young's modulus of the PLLA film (Fig. S9 online). The piezoelectricity of the pcm-PLLA scaffolds came from the PLLA fibers, which had the largest piezoelectric output in the d_{14} direction. We hypothesized that the modified HA particles would have a shielding effect on the piezoelectric signal [39]. Subsequently, we evaluated the piezoelectric performance of each scaffold, including voltage output under ultrasound, d_{14} piezoelectric coefficient, and PFM test (Fig. 2j, k and Fig. S10 online). PLA scaffold had almost no piezoelectricity, while the PLLA scaffold had a voltage output of about 220 mV. With increasing HA thickness, the output voltage of the pcm-PLLA gradually decreased

Please cite this article as: X. Cui, L. Xu, Y. Shan et al., Piezocatalytically-induced controllable mineralization scaffold with bone-like microenvironment to achieve endogenous bone regeneration, Science Bulletin, https://doi.org/10.1016/j.scib.2024.04.002

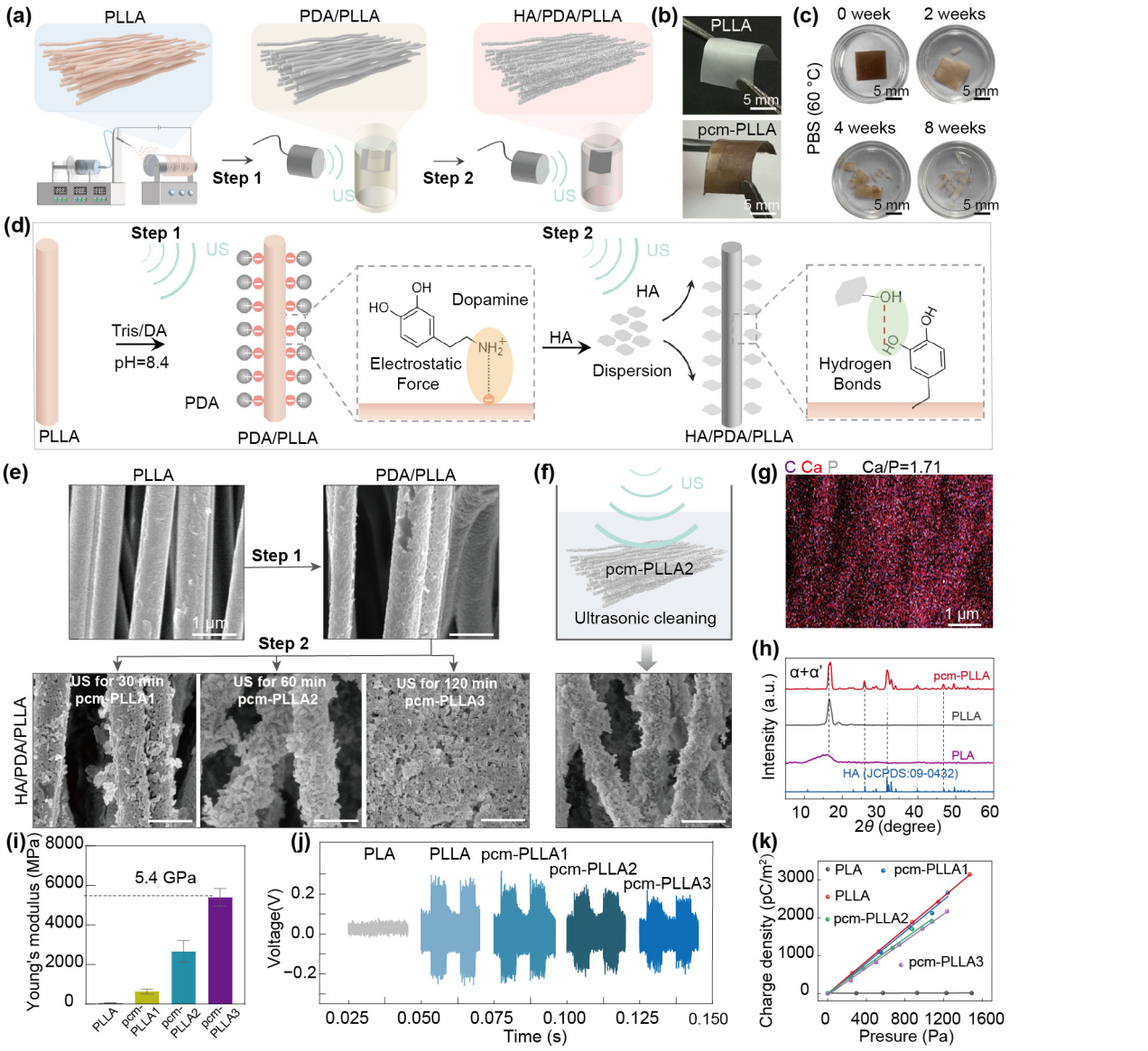

Fig. 2. Preparation and characterization of piezocatalytically-induced controllable mineralization PLLA scaffold (pcm-PLLA). (a) Schematic diagram of the synthesis process of pcm-PLLA. (b) Physical representation of PLLA and pcm-PLLA. (c) Accelerated degradation experiments of pcm-PLLA in PBS. (d) Schematic diagram of the synthesis principle of pcm-PLLA. (e) Surface SEM images of PLLA, PDA/pcm-PLLA and different HA modification times for HA/PDA/PLLA. (f) SEM image of the surface of pcm-PLLA2 after ultrasonic cleaning for 30 min. (g) Distribution of elemental mapping of C, Ca and P of pcm-PLLA. (h) XRD characterization of the scaffolds. The standard card number for HA is JCPDS:09-0432. (i) Young's modulus results of different scaffolds by AFM. (j) Voltage output of pcm-PLLA scaffolds with different thicknesses of HA under ultrasound. (k) Piezoelectric coefficients of pcm-PLLA scaffolds with different thicknesses of HA in the d_{14} direction.

to about 210, 190, and 180 mV, respectively (Fig. 2j). The d_{14}-direction piezoelectric coefficient of PLLA was 2.21 pC/N, while the piezoelectric coefficients of the pcm-PLLA scaffolds were reduced in the order of 1.99, 1.82, and 1.66 pC/N (Fig. 2k). To ensure a balance among the morphology, mechanical and electrical properties of pcm-PLLA scaffolds, we selected pcm-PLLA2 for the following experiments.

3.2. Osteogenic differentiation potentials of MSCs on bionic piezoelectric pcm-PLLA scaffold in vitro

The physical and chemicals clues of scaffolds, including morphology, mechanics, electricity, and chemistry may significantly affect cell migration, adhesion, morphology, proliferation, differentiation, and thus regulate the fate of MSCs osteogenic differentiation (Fig. 3a). To elucidate the cellular effects of the pcm-PLLA scaffold, MSCs were seeded on different scaffolds, including PLA, PLLA, and pcm-PLLA, with tissue culture plastic (TCP) as a blank group. Phalloidin staining of MSCs grown on the surface of the scaffolds for 12 and 48 h showed that the pcm-PLLA scaffold displayed better cell adhesion ability than TCP and promoted the proliferation of MSCs in the short term (Fig. 3b, i and Fig. S11 online). Cell activity was also assayed with counting Kit 8 (CCK8) (Fig. 3j). In addition, the orientation of the cells and fibers was highly consistent (Fig. 3c and Fig. S12 online). The 3D images taken by laser confocal (Fig. 3d, e) showed that the cell could also grow rapidly into the interior of the scaffolds 20 μm 12 h after being seeded. SEM image also showed that the cells could grow into the interior of the scaffold with more tentacles (Fig. 3f). Vinculin proteins are membrane proteins with important roles in cell adhesion functions [2,3,40]. Cells on TCP limited spreading and distribution of vinculin (Fig. S13 online), in contrast, much more focal adhesion was

Please cite this article as: X. Cui, L. Xu, Y. Shan et al., Piezocatalytically-induced controllable mineralization scaffold with bone-like microenvironment to achieve endogenous bone regeneration, Science Bulletin, https://doi.org/10.1016/j.scib.2024.04.002

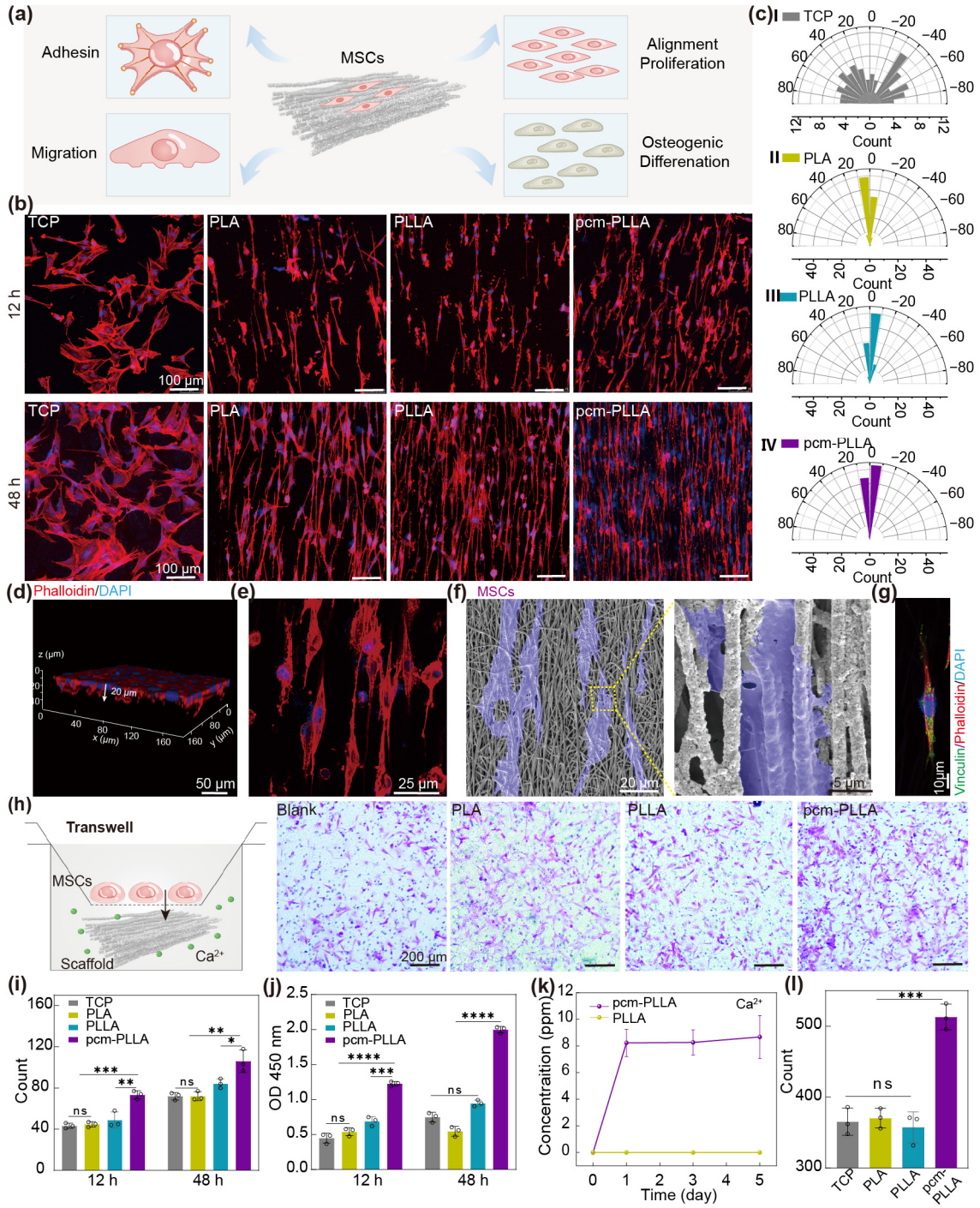

Fig. 3. Biological effects of pcm-PLLA scaffolds on MSCs. (a) pcm-PLLA scaffolds affect MSCs in adhesion, migration, proliferation and differentiation. (b) Growth of MSCs staining on different substrates by phalloidin and DAPI (12 and 48 h) (red: Phalloidin, F-actin; blue: DAPI, nucleus). (c) Statistics on the directionality of MSCs growth on different substrates (48 h). (d, e) 3D and planar images of MSC with phalloidin (red: F-actin) and DAPI (blue: nucleus) staining (12 h). (f) SEM images of MSC grown on pcm-PLLA scaffolds. (g) Vinculin (green: vinculin) phalloidin (red: F-actin) and DAPI (blue: nucleus) staining of MSCs on pcm-PLLA. (h) Schematic of transwell and pictures of crystal violet staining (purple) of MSCs. (i) Statistical plot of the number of cells in each field of view (0.45 mm^2) for Fig. 3b, $n = 3$. (j) Cell viability of MSCs grown on different substrates at 12 and 48 h. (k) Ca^{2+} release profiles of PLLA and pcm-PLLA scaffolds in saline. (l) Statistical plot of the number of cells in each field of view (1.44 mm^2) for Fig. 3h, $n = 3$.

expressed in the pcm-PLLA group marked by vinculin–fluorescein isothiocyanate (FITC) (Fig. 3g). These results showed that MSCs were better able to adhere to the pcm-PLLA scaffold for directed growth and with more tentacles, which are considered to be favorable for osteogenic differentiation [29,41]. To explore the effect of pcm-PLLA scaffolds on cell migration and recruitment, transwell assay was performed. As shown in Fig. 3h, MSCs were planted in the upper chamber and different scaffolds were placed in the lower chamber, cells that migrated to the lower chamber were counted at the same time (Fig. 3h). The statistical results showed that pcm-PLLA could significantly promote the migration of MSCs (Fig. 3l). In this regard, we suspected that the pcm-PLLA scaffolds were able to slowly release Ca^{2+} thereby providing a chemical environment more conducive to the growth and differentiation of MSCs [42].

Please cite this article as: X. Cui, L. Xu, Y. Shan et al., Piezocatalytically-induced controllable mineralization scaffold with bone-like microenvironment to achieve endogenous bone regeneration, Science Bulletin, https://doi.org/10.1016/j.scib.2024.04.002

The results of Ca^{2+} release experiments with the scaffolds also confirmed this (Fig. 3k).

To test the effect of the electrical environment provided by the pcm-PLLA scaffold on the osteogenic differentiation of MSCs, ultrasound was used to activate the piezoelectric signals of the pcm-PLLA scaffold. According to the results of CCK8, the activity of the cells showed a decreasing trend with increasing ultrasound intensity (Fig. S14 online). And the cells on the surface of TCP showed a more sensitive response. To ensure that the cell activity was above 90%, the ultrasound intensity chosen for subsequent experiments was 0.8 W/cm^2. The frequency of ultrasound interventions was 1 min and twice a day [22,43].

Cellular calcium ion content is highly relevant to osteogenic differentiation [7,14,15]. Electrical signals can increase intracellular calcium content by opening the calcium ion channel, thus further activating the expression of osteogenic proteins such as ALP, Runt-related transcription factor 2 (Runx2), Col I, and osteocalcin (OCN) [44], and ultimately affecting osteogenesis differentiation (Fig. 4a). We planted MSCs on the surface of pcm-PLLA scaffold and performed fluorescence staining of intracellular calcium ions using the calcium fluorescent probe Fluo-4 AM. Momentary ultrasound was applied to the pcm-PLLA scaffold at the 5th second, and the fluorescence intensity of MSCs on the pcm-PLLA scaffold was observed to rose rapidly and persisted for 50 s, but there was no significant change in the fluorescence intensity of cells on the TCP (Fig. 4b, c, Movie S1 and Fig. S15 online). The short-term decrease in fluorescence intensity was caused by the mechanical vibration of the material induced by ultrasound, which causes the cell position to deviate from the focal position. These results indicated that piezoelectricity triggered by ultrasound can transiently activate voltage-dependent calcium channels in the cell membrane, resulting in a significant increase in the level of calcium influx.

In order to observe the long-term effects of piezoelectricity on osteogenic differentiation of MSCs, we identified the relative expression of osteogenesis-related proteins and genes by immunofluorescence staining and qPCR, respectively. The experiments were divided into 8 groups: TCP, PLA, PLLA, and pcm-PLLA, as well as these four groups with the addition of ultrasound. The detection time points were day 3 and 7 after changing the osteogenic differentiation medium. ALP is a protein expressed at the early stage of osteogenic differentiation which marks the beginning of differentiation [45]. According to Fig. S16 (online), the results of ALP quantitative test on day 3 showed that the expression of TCP, PLA, PLLA groups were not obvious, but the expression of pcm-PLLA group and pcm-PLLA + US group was significantly increased, which indicated that in the early stage, HA in pcm-PLLA scaffolds acted as a switch to turn on the osteogenic differentiation [13,46,47]. At day 7, ALP expression was higher in pcm-PLLA + US group than that in pcm-PLLA group, and higher in PLLA + US group than that in PLLA group, suggesting that ultrasonic piezoelectricity consistently promotes osteogenic differentiation. In immunofluorescence staining experiments, the characteristic functional proteins of osteoblasts, BMP2, and OCN, were stained with fluorescence and semi-quantitatively counted (Fig. 4d and e, Fig. S17 online). At day 7, MSCs grown on pcm-PLLA scaffold expressed higher protein after US intervention. Notably, protein expression was also higher in the PLLA group without US than that in PLA group, which was attribute to the piezoelectricity of the scaffolds triggered by cells during growth and migration [6]. To quantify the expression of each gene in the cells, we quantified the expression of osteogenic-related genes (ALP, Runx2, Col I, and OCN) using qPCR on day 3 (Fig. 4f) and day 7 (Fig. S18 online). The expression of these genes gradually increased over time, with the highest expression in the pcm-PLLA + US group.

3.3. Cell homing of endogenous stem cells by pcm-PLLA

Migration of endogenous stem cells to the site of bone defects is a critical step for bone repair [36,37,48], and we validated the ability of pcm-PLLA scaffolds to recruit endogenous stem cell *in vivo* in a rat model of skull bone defects (Fig. 5a). Specifically, we created a circular bone defect with a diameter of 5 mm in the skull of rats, and then filled with scaffolds by using the UV-cured hydrogel (Fig. 5b). Ten days later, the defect site was harvested and stained with H&E. As shown in Fig. 5d, the PLA scaffold without annealing had lost its fibrous structure to become a dense membrane *in vivo* due to unstable crystallinity. Compared with the other groups, the cells in the pcm-PLLA group were grew directionally and tightly aligned along the direction of the fibers in pcm-PLLA scaffold, which provided a direction for subsequent mineralization (Fig. 5d). The cell counts within the field of view were meticulously recorded. In the Blank, PLA, and PLLA groups, the cell numbers were found to be 622, 701, and 796, respectively. Notably, the pcm-PLLA group exhibited a significantly higher cell count, with a total of 1963 cells, markedly surpassing the other groups (Fig. 5c). The pcm-PLLA scaffold's porous structure and suitable chemical environment facilitated the rapid recruitment of endogenous stem cells, resulting in successful osseointegration.

We performed immunofluorescence staining for osteoinductive markers to confirm whether the recruited cells were endogenous MSCs (BMP2, OCN, and Runx2). There are three stages of differentiation of MSCs: proliferation, matrix maturation, and matrix mineralization. Early differentiation stage was characterized by high expression of BMP2 and Runx2, and later stage was characterized by elevated expression of extracellular matrix proteins, such as OCN [44]. Cells in each scaffold showed fluorescent expression, but the strongest fluorescent was expressed in pcm-PLLA group, indicating that the majority of the recruited cells were MSCs and showed better osteogenic capacity (Fig. 5e, Fig. S19 online). The semiquantitative statistics of fluorescence are also shown in Fig. 5f. Interestingly, the fluorescence intensity was stronger at the edge of the scaffold than that inside the scaffold, indicating that the cells gradually migrated from the surface into the interior of the scaffold and differentiated towards osteoblasts.

We further explored the effect of the scaffold on the inflammatory environment and angiogenesis at the defect site. M1 ($CD86^+$) and M2 ($CD206^+$) type macrophages are common pro-inflammatory and anti-inflammatory cells, which are essential for regulating the osteogenic microenvironment. Short-term inflammatory environments are favorable for recruitment of endogenous stem cells, but longer-term inflammatory environments are detrimental to the bone repair process. Compared with the other groups, cells in the pcm-PLLA scaffolds showed 86% M2 (red) and 13% M1 (green) macrophages, indicating a favorable bone repair environment (Fig. 5i, g and Fig. S20 online). We further evaluated the expression of vascular endothelial growth factor (VEGF) by immunohistochemistry (IHC) to observed scaffold-mediated angiogenesis (Fig. 5j, h). Angiogenesis was observed in all groups, but the vessel density was significantly higher in the pcm-PLLA group. Along with the inflammatory characterization results, it demonstrated that the pcm-PLLA scaffold provided a favorable osteogenic microenvironment.

3.4. Pcm-PLLA achieved endogenous bone regeneration in the rat skull defect model

The process of bone regeneration is divided into three stages: first, in the early stage of bone defect, endogenous MSCs are recruited by the scaffold; second, the proliferation and differentiation of MSCs are stimulated by ultrasound piezoelectricity; finally, osteoblasts are further mature and mineralize into bone tissue

Please cite this article as: X. Cui, L. Xu, Y. Shan et al., Piezocatalytically-induced controllable mineralization scaffold with bone-like microenvironment to achieve endogenous bone regeneration, Science Bulletin, https://doi.org/10.1016/j.scib.2024.04.002

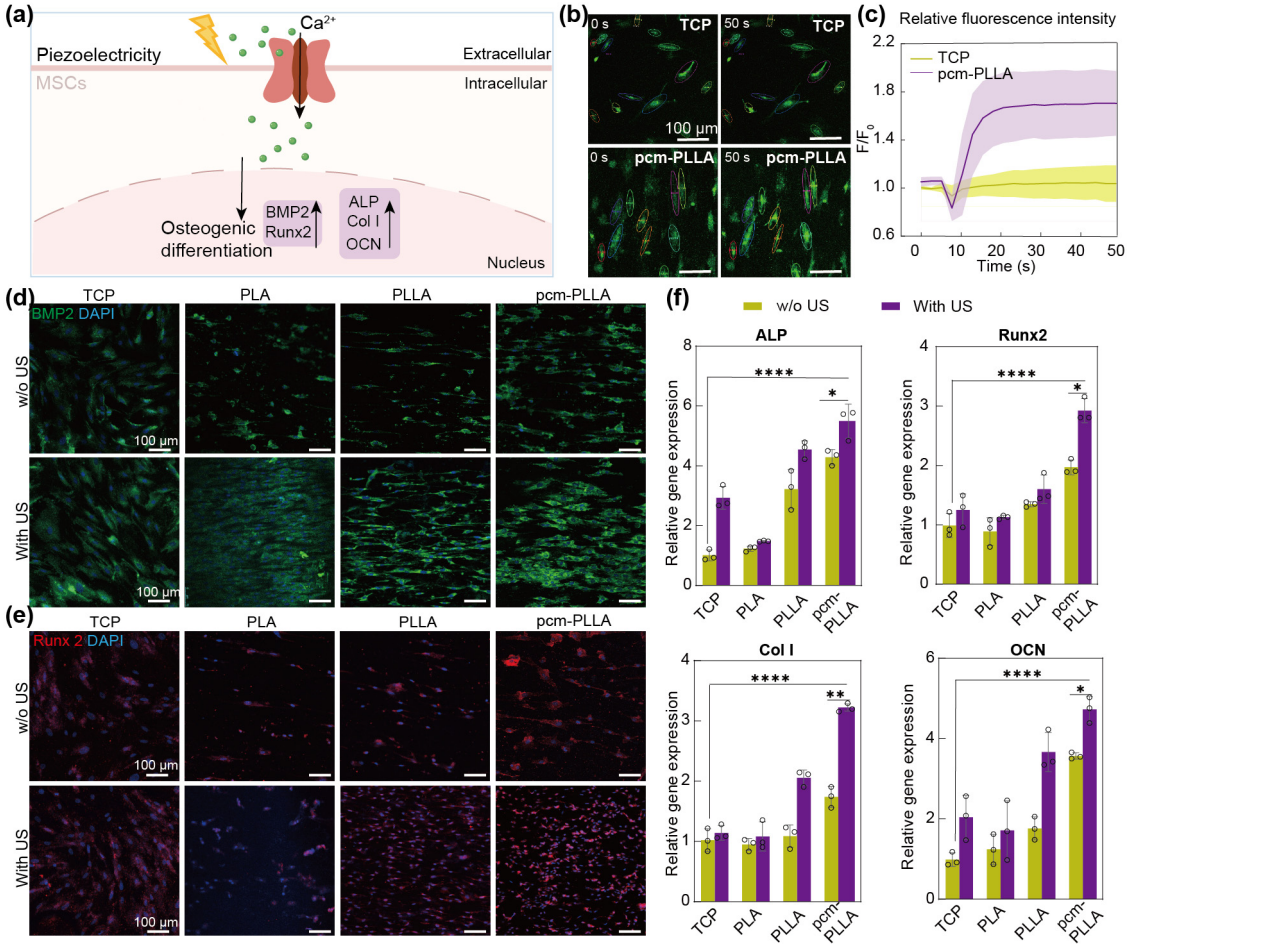

Fig. 4. Biological effects of piezoelectricity of pcm-PLLA on MSCs. (a) Piezoelectricity promoted the opening of Ca^{2+} channels in MSCs resulting in a rapid increase in intracellular Ca^{2+} concentration thereby promoting the expression of osteogenesis-related genes. (b) Pictures of intracellular Ca^{2+} fluorescence staining of MSCs. (c) Relative fluorescence intensity of intracellular Ca^{2+} fluorescence in MSCs over time. (d, e) IF staining of MSCs for BMP2 and OCN. (f) qPCR of osteogenesis-related genes in MSCs (3 days).

(Fig. 6a, b). *In situ* bone regeneration is the most direct way to evaluate the effect of scaffolds bone repair.

At 4 weeks after implantation, micro-CT images (Fig. 6c and Fig. S21 online) and corresponding semi-quantitative results (Fig. 6d, e and Fig. S22 online) showed that only a small amount of new bone was generated along the margins in the Blank and PLA groups, with new bone area of 15.3% ± 2.3% and 14.5% ± 0.9% respectively, indicating that the physical support of PLA did not significantly promote bone formation. More than half of the defects were covered by new bone in the PLLA group (54% ± 2.9%), in part because of the piezoelectric signals by the growth and migration of cells. The new bone formed in the pcm-PLLA group (81.9% ± 3.7%) was further increased compared with the PLLA group, confirming the role of chemical environment from HA. While the coverage of bone was close to 100% in the pcm-PLLA + US group (87.9% ± 1.6%), indicating that ultrasound activated the osteogenic differentiation of MSCs and further promoted the process of bone repair. The bone volume/tissue volume (BV/TV) results of the newly formed bone were generally consistent with the trend of the newly formed bone area (Fig. 6e). At 12 weeks, the thickness of the new bone in the pcm-PLLA + US group was already almost the same as that of the original bone (BV/TV = 94.4% ± 3.1%). In order to comprehensively analyze the role of various factors in the process of bone formation, we further compared the bone repair effects of Blank, PLA and PLLA groups with and without ultrasound. According to Fig. S21 (online), ultrasound did not increase the new bone in the Blank + US and PLA + US groups, indicating that ultrasound alone had no obvious biological effect. PLLA + US (BV/TV = 74.5% ± 2.3%) group showed a 3.8% increase in BV/TV compared to the PLLA (BV/TV = 70.7% ± 1.7%) group, and the pcm-PLLA + US (BV/TV = 94.4% ± 3.1%) group showed a 12% increase in BV/TV compared with the pcm-PLLA (BV/TV = 82.4% ± 3.1%) group. Ultrasound played a more significant role in the pcm-PLLA group. In conclusion, the chemical environment for recruiting cells, the appropriate structural, mechanical properties and the electrical environment are all essential for bone regeneration.

Next, regenerative sections were studied by MT (Fig. 6f), H&E (Fig. S23 online), and BMP2, OCN, Runx2 IF staining (Fig. S24 online). MT staining showed that there was only a small amount of new bone tissue at the edge of the defect in the Blank and PLA groups, and there was a little collagen at the defect site. In the PLLA group, there was a large amount of collagen inside the scaffold, indicating more osteoblasts and fibroblast infiltrated it. In the pcm-PLLA group, mature bone tissue was observed, while in the pcm-PLLA + US group, the defect was almost completely filled with new bone tissue which tightly integrated with the old bone. According to the result of H&E staining, there was no scaffold observed, which had been completely replaced by new bone.

In addition, immunofluorescence staining (BMP2, OCN, and Runx2) was performed 12 weeks after implantation to examine the osteogenic activity at the site of defects. In Blank and PLA groups, only a small amount of protein was expressed, while a

Please cite this article as: X. Cui, L. Xu, Y. Shan et al., Piezocatalytically-induced controllable mineralization scaffold with bone-like microenvironment to achieve endogenous bone regeneration, Science Bulletin, https://doi.org/10.1016/j.scib.2024.04.002

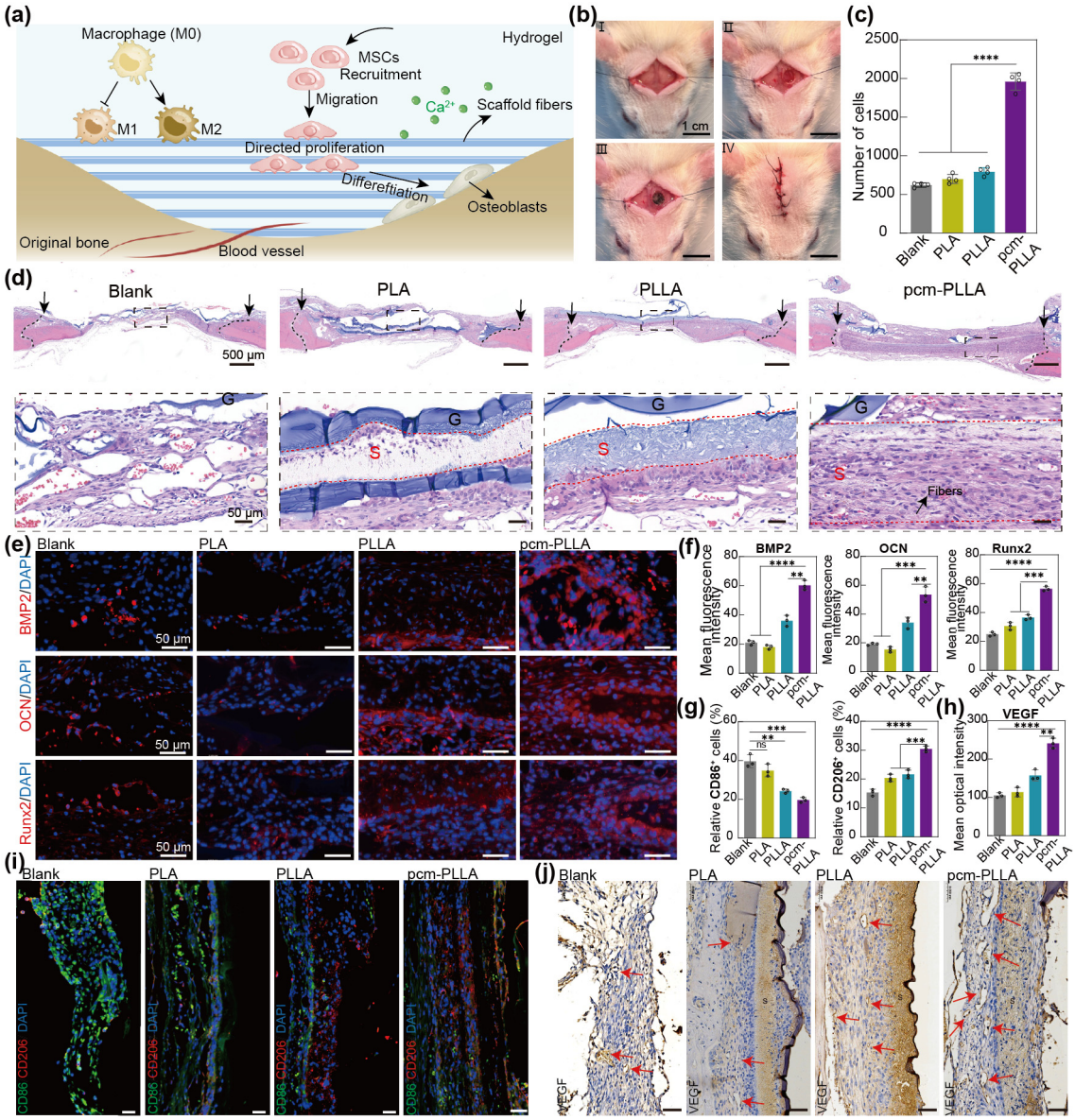

Fig. 5. Biological effects of pcm-PLLA scaffolds 10 days after implanted *in vivo*. (a) Schematic representation of the biological effects of pcm-PLLA scaffolds *in vivo*. (b) pcm-PLLA scaffold implantation procedure. (c) A statistical plot of the number of cells in the field of view (0.25 mm^2) in Fig. 5d. (d) HE staining of the bone defect 10 days after implanted (S: scaffold; G: hydrogel). (e) Immunofluorescence staining for BMP2, OCN, and Runx2 in the bone defects 10 days after implanted. (f) Semi-quantitative counting of fluorescence in Fig. 5e. (g) Semi-quantitative counts of fluorescence for CD86 (M1) and CD206 (M2) positive cells in Fig. 5i. (h) Semi-quantitative counting of VEGF-positive regions in Fig. 5j. (i) IF staining for CD86 and CD206 at the site of a bone defect 10 days after implanted (scale bar = 50 μm). (j) IHC staining of VEGF at the site of bone defects (scale bar = 50 μm).

large number of marker proteins were expressed in PLLA, PLLA + US, and pcm-PLLA groups, which indicated the middle and late process of osteogenic differentiation. However, in pcm-PLLA + US group, bone regeneration was almost completed, so only a small amount of protein was expressed. The body weights of the rats recorded during the treatment and the H&E staining results of the vital organs at the end of the treatment both demonstrated the biosafety of the scaffold (Figs. S25 and 26 online).

3.5. The osteogenic differentiation mechanism of pcm-PLLA by transcriptomic analysis

The transcriptomics of bone defect tissues from the Ctrl, PLA + US, and pcm-PLLA + US groups were analyzed to explore the mechanism of osteogenic differentiation. Firstly, according to the upset plot it showed that there were differences in the gene sets between the groups (Fig. 7a). The one-way analysis of variance for correlation for each sample group was within acceptable limits, and the different groups also showed significantly different sets of genes (Fig. 7b). Differential genes in the pcm-PLLA + US group and the Ctrl group were then analyzed in circus (Fig. 7c). The results showed that, comparing with the Ctrl group without scaffold implantation, the main differentially expressed genes in the pcm-PLLA + US group were enriched in the relevant pathways as shown in the figure, among which those related to osteogenic differentiation were PI3K-Akt signaling pathway. Ctrl, PLA + US, and pcm-PLLA + US groups were compared two by two thus obtaining the differential gene (Fig. 7d, e). The heatmaps showed the differential genes upregulated by pcm-PLLA + US. Differential genes are labeled in Volcano (Fig. 7h, k), which include genes related to cell adhesion

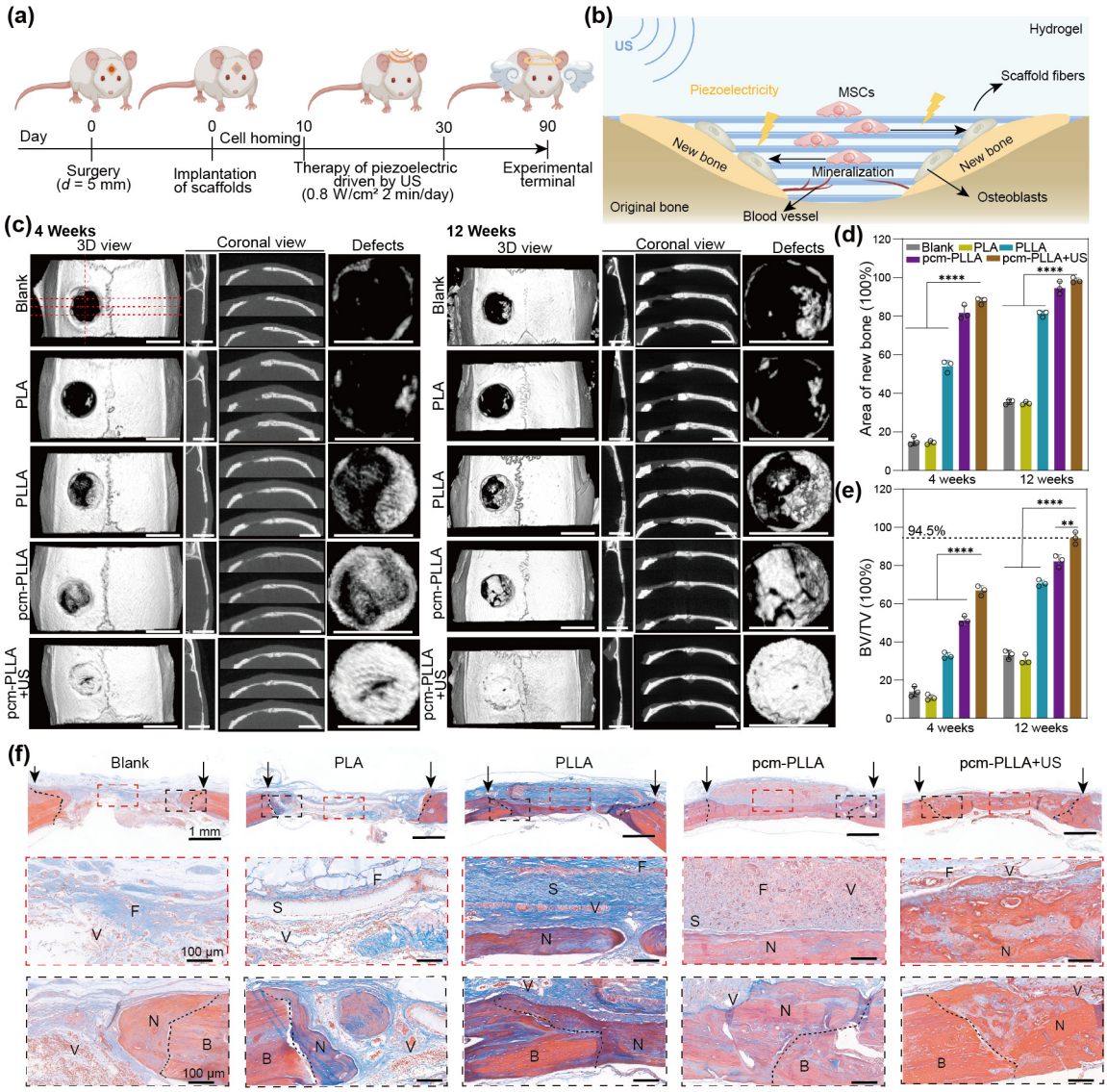

Fig. 6. Long-term bone repair effects of pcm-PLLA scaffolds *in vivo*. (a) Schematic diagram of the surgery and treatment process. (b) *In vivo* biological effects of scaffolds under ultrasound piezoelectricity. (c) CT images of rat cranial bone (scale bar = 5 mm). (d) Area of the new bone at different times. (e) New BV/TV of rat skull bone at different times. (f) MT staining of the bone defect site after 12 weeks. The black arrow points to the junction of the old and new bone (S: scaffolds; V: new vessels; B: old bone; N: new bone; F: collagen fibers).

(Ibsp, Itgb2, Nrcam), osteogenic differentiation (Bmp3, Mmp9), osteogenic mineralization (Slc26a9, Vdr), NF-κB signaling pathways (Lyn, Plau), and angiogenesis (Tgfbr1).

The relevant top enriched up-KEGG pathways speculated that pcm-PLLA + US further promoted cell adhesion and proliferation (protein digestion and absorption, focal adhesion) and also polarization of M2-type macrophages (NF-κB signaling pathways). Further, the pcm-PLLA + US group also regulated stem cell proliferation (Cytokine-cytokine receptor interaction) as well as osteogenic differentiation (PI3K-Akt signaling pathway) (Fig. 7f, g). The GO database analysis of the differential genes further demonstrated a better bone-enhancing effect in the pcm-PLLA + US treatment group (Fig. 7i, j). Compared with the PLA + US group without piezoelectricity or HA nanoparticles, the pcm-PLLA + US treatment group promoted osteogenic differentiation and mineralization (bone mineralization, biomineral tissue development, and positive regulation of cell differentiation) by promoting stem cell proliferation (regulation of MAPK cascade), angiogenesis (blood vessel diameter maintenance and blood circulation) and anti-inflammatory aspects (positive regulation of immune system process). Transcriptomics data analysis showed that pcm-PLLA + US accelerated stem cell recruitment, angiogenesis, and the formation of an anti-inflammatory environment through the integration of HA nanoparticles and piezoelectricity.

4. Discussion and conclusion

In recent years, significant progress has been made in the research of electroactive bone implant materials. Piezoelectric materials have gained widespread attention as one of the ideal candidates for electroactive bone implant materials; however, their mechanical strength, osseointegration, biocompatibility, and biodegradability have become limitations for their clinical applications in orthopedics. Here, we present a biomimetic piezoelectric pcm-PLLA fibrous scaffold with PLLA as the main electroactive component. HA, as a major inorganic constituent of bone, has been shown to upregulate the endoplasmic reticulum calcium ATPase (adenosine triphosphatase) subunits, ATP2A2 and ATP2B2, and

Please cite this article as: X. Cui, L. Xu, Y. Shan et al., Piezocatalytically-induced controllable mineralization scaffold with bone-like microenvironment to achieve endogenous bone regeneration, Science Bulletin, https://doi.org/10.1016/j.scib.2024.04.002

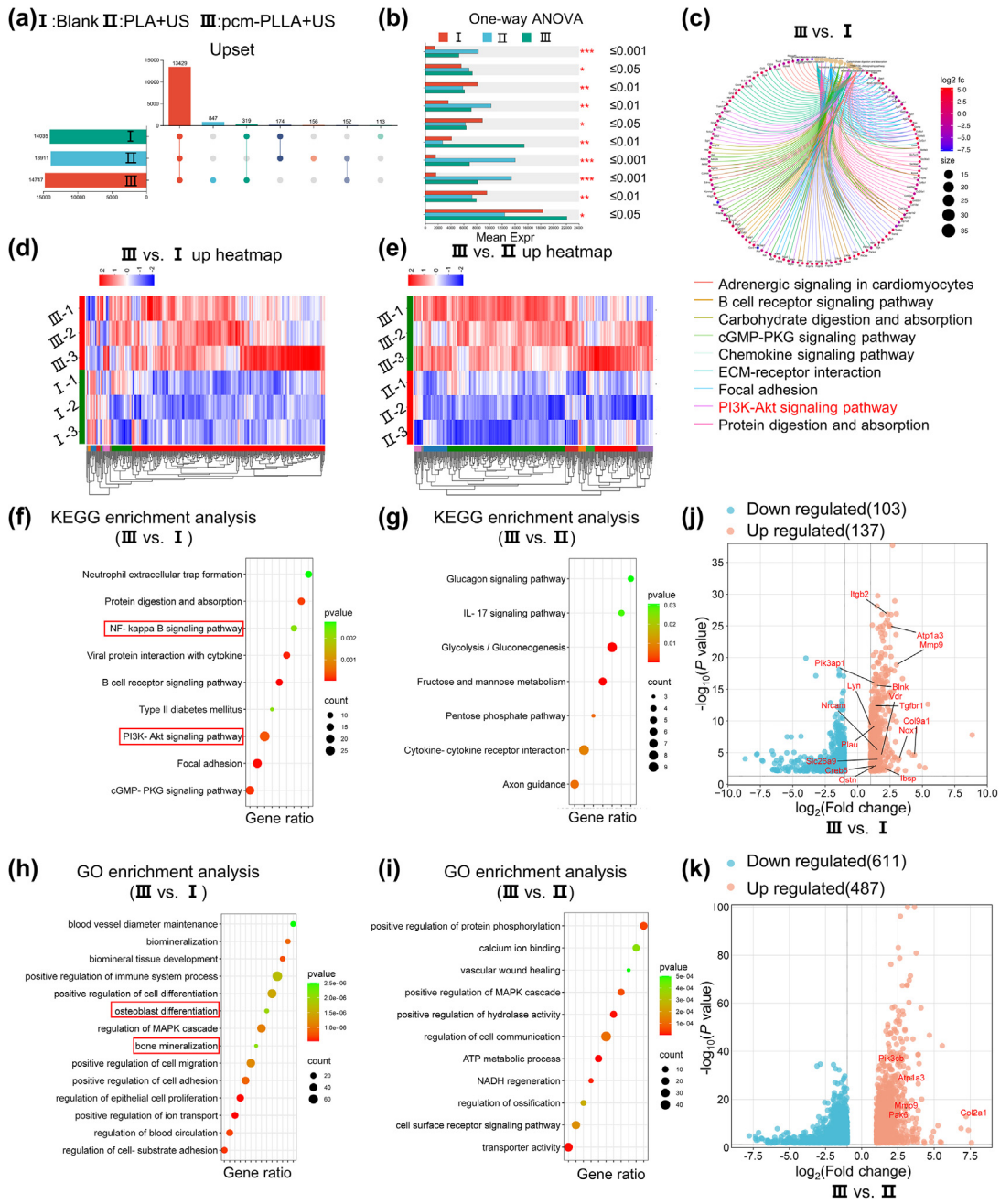

Fig. 7. Transcriptome test of neoplastic tissue at 4 weeks after implanted. (a) Upset plots of shared and unique genes between groups. (b) Correlation analysis plot of differential genes between groups. (c) Differential gene circle map of the pcm-PLLA + US group relative to the Ctrl group. (d) Differential gene enrichment heatmaps for the pcm-PLLA + US group relative to the Ctrl group, and (e) relative to the PLA + US group, and associated gene annotations. (f) Bubble plots of KEGG enrichment of differential genes in the pcm-PLLA + US group relative to the control group, and (g) relative to the PLA + US group. (h) Bubble plots of GO enrichment of differential genes in the pcm-PLLA + US group relative to the Ctrl group, and (i) relative to the PLA + US group. (j) Volcano maps of differential gene enrichment in the pcm-PLLA + US group relative to the Ctrl group, and (k) relative to the PLA + US group.

thus promote osteogenesis [7,18]. PLLA is a polymer with good biocompatibility that has been validated for use as a bone implant material [49]. Therefore, inspired by the natural bone structure, we uniformly modified HA particles on the surface of PLLA fibrous scaffolds. HA modified on the surface not only changes the ionic environment in the scaffold microenvironment, but also provides more suitable morphological characteristics for cell adhesion and proliferation. It is worth mentioning that this strategy of modifying HA on the surface of PLLA fibers retains the piezoelectricity of PLLA better than mixing them directly [30,33]. And during the preparation of the scaffolds, PDA was modified as a bridging layer between HA and PLLA. We innovatively used ultrasound to facilitate the modification of PDA, and compared with the traditional modification method, the 3D structure of the scaffolds was better preserved and the modification time was greatly reduced [35].

In vitro experiments have shown that pcm-PLLA can promote the adhesion, migration, orientation and proliferation of MSCs. In addition, ultrasound-induced electrical signals on the surface of

the scaffold significantly promoted the opening of voltage-gated Ca^{2+} channels on the cell membrane, leading to a significant increase in intracellular Ca^{2+} influx and accelerated osteogenic differentiation. *In vivo* experiments showed that on the 10th day after scaffold implantation, stem cells were significantly aggregated within the pcm-PLLA scaffolds, the macrophage M1/M2 ratio decreased, and angiogenesis increased significantly. Therefore, the scaffold can rapidly recruit stem cells at the early stage of bone repair and improve the immune microenvironment of the bone defect site, which is necessary for subsequent bone repair. The skull defect site in the pcm-PLLA + US group was almost completely covered by new bone after 4 weeks postoperatively, suggesting that piezoelectric scaffold can greatly shorten the duration of the treatment of bone defects. From the results of animal tissue transcriptome, the piezoelectric pcm-PLLA scaffolds significantly increased cell migration, adhesion (protein digestion and absorption, focal adhesion) and polarization of M2-type macrophages (NF-κB signaling pathways). We hypothesize that pcm-PLLA causes cell adhesion and migration because the extracellular matrix of cells can adsorb to the surface of HA nanoparticles to form adhesion protein structural domains, which promotes the expression of cellular integrins to achieve cell adhesion. Furthermore, the pcm-PLLA scaffold is able to fast-track the initiation of angiogenesis (blood vessel diameter maintenance and blood circulation) and osteogenesis (bone mineralization, biomineral tissue development and positive regulation of cell differentiation), which correlated with the up-regulated expression of M2. Rapid angiogenesis is thought to be synergistic with VEGF secretion by M2-type macrophages. Furthermore, in the pcm-PLLA + US treatment group, the PI3K-Akt signaling pathway was significantly up-regulated, which is thought to be a possible key signaling pathway in piezoelectricity-promoted osteogenic differentiation.

In summary, we have established a bionic pcm-PLLA scaffold with a bone-like microenvironment. The following innovations are presented: (1) Controlled mineralization rapidly achieved by piezoelectric catalysis. (2) pcm-PLLA scaffold recruits endogenous stem cells thus leading to rapid osseointegration, which is essential for the subsequent bone regeneration. (3) Ultrasound piezoelectricity and bone-like morphology, mechanical and chemical properties of pcm-PLLA scaffold promote bone regeneration processes including osteogenic differentiation, M2 macrophage polarization and angiogenesis. (4) This pcm-PLLA scaffold degrades at a rate consistent with the rate of new bone production. The scaffold with a bone-like microenvironment not only informs the development of bone regeneration scaffolds, but also has great potential for clinical transformation.

Conflict of interest

The authors declare that they have no conflict of interest.

Acknowledgments

This work was supported by Beijing Natural Science Foundation (L212010), the National Natural Science Foundation of China (T2125003, 52372174), the New Cornerstone Science Foundation, Major Instrument Project of the National Natural Science Foundation of China (22027810), and the National Key Research and Development Program of China (2022YFB3804703, 2022YFE0111700, 2021YFA1200900, 2021YFB3201204, 2022YFB3205602).

Author contributions

Dan Luo, Chunying Chen, and Zhou Li were responsible for the experimental concept and design. Xi Cui, Lingling Xu, Yizhu Shan, and Jiaxuan Li designed the study. Xi Cui, Jiaxuan Li, Jianying Ji, Engui Wang, Xiaozhou Wen, Yuan Bai performed experimental measurement and data analyses. Xi Cui, Lingling Xu, Yizhu Shan, Jianying Ji, and Baokun Zhang took and processed the experimental photograph and video. Xi Cui and Lingling Xu wrote the original draft. Dan Luo, Chunying Chen, and Zhou Li were responsible for project administration, conceptualization, supervision, funding acquisition, validation and review. All authors discussed the results and commented on the manuscript.

Appendix A. Supplementary material

Supplementary material to this article can be found online at https://doi.org/10.1016/j.scib.2024.04.002.

References

[1] Zhu GY, Zhang TX, Chen M, et al. Bone physiological microenvironment and healing mechanism: Basis for future bone-tissue engineering scaffolds. Bioact Mater 2021;6:4110–40.
[2] Singh S, Nyberg EL, O'Sullivan AN, et al. Point-of-care treatment of geometrically complex midfacial critical-sized bone defects with 3D-printed scaffolds and autologous stromal vascular fraction. Biomaterials 2022;282:121392.
[3] Wei HP, Cui JJ, Lin KL, et al. Recent advances in smart stimuli-responsive biomaterials for bone therapeutics and regeneration. Bone Res 2022;10:17.
[4] Hench LL, Polak JM. Third-generation biomedical materials. Science 2002;295:1014–7.
[5] Koons GL, Diba M, Mikos AG. Materials design for bone-tissue engineering. Nat Rev Mater 2020;5:584–603.
[6] Liu ZR, Wan XY, Wang ZL, et al. Electroactive biomaterials and systems for cell fate determination and tissue regeneration: Design and applications. Adv Mater 2021;33:2007429.
[7] Stevens MM. Biomaterials for bone tissue engineering. Mater Today 2008;11:18–25.
[8] Wei S, Wang F, Zou X, et al. Flexible quasi-2D perovskite/IGZO phototransistors for ultrasensitive and broadband photodetection. Adv Mater 2020;32:1907527.
[9] Zhu LS, Luo D, Liu Y. Effect of the nano/microscale structure of biomaterial scaffolds on bone regeneration. Int J Oral Sci 2020;12:6.
[10] Yang ZJ, Yuan HP, Tong WD, et al. Osteogenesis in extraskeletally implanted porous calcium phosphate ceramics: Variability among different kinds of animals. Biomaterials 1996;17:2131–7.
[11] Minary-Jolandan M, Yu MF. Uncovering nanoscale electromechanical heterogeneity in the subfibrillar structure of collagen fibrils responsible for the piezoelectricity of bone. ACS Nano 2009;3:1859–63.
[12] Yuan B, Zhang YX, Zhao R, et al. A unique biomimetic modification endows polyetherketoneketone scaffold with osteoinductivity by activating cAMP/PKA signaling pathway. Sci Adv 2022;8:eabq7116.
[13] Yuan B, Wang LN, Zhao R, et al. A biomimetically hierarchical polyetherketoneketone scaffold for osteoporotic bone repair. Sci Adv 2020;6:eabc4704.
[14] Nakade O, Takahashi K, Takuma T, et al. Effect of extracellular calcium on the gene expression of bone morphogenetic protein-2 and-4 of normal human bone cells. J Bone Miner Metab 2001;19:13–9.
[15] Barradas AMC, Fernandes HAM, Groen N, et al. A calcium-induced signaling cascade leading to osteogenic differentiation of human bone marrow-derived mesenchymal stromal cells. Biomaterials 2012;33:3205–15.
[16] Fu J, Liu X, Tan L, et al. Photoelectric-responsive extracellular matrix for bone engineering. ACS Nano 2019;13:13581–94.
[17] Siddappa R, Martens A, Doorn J, et al. cAMP/PKA pathway activation in human mesenchymal stem cells *in vitro* results in robust bone formation *in vivo*. Proc Natl Acad Sci USA 2008;105:7281–6.
[18] Tang ZR, Chen SY, Ni YL, et al. Role of Na^+, K^+-ATPase ion pump in osteoinduction. Acta Biomater 2021;129:293–308.
[19] Li J, Du HR, Ji X, et al. ETV2 promotes osteogenic differentiation of human dental pulp stem cells through the ERK/MAPK and PI3K-Akt signaling pathways. Stem Cell Res Ther 2022;13:495.
[20] Bohner M, Miron RJ. A proposed mechanism for material-induced heterotopic ossification. Mater Today 2019;22:132–41.

[21] Jakus AE, Rutz AL, Jordan SW, et al. Hyperelastic "bone": A highly versatile, growth factor–free, osteoregenerative, scalable, and surgically friendly biomaterial. Sci Transl Med 2016;8:358ra127.
[22] Lei J, Wang CF, Feng XB, et al. Sulfur-regulated defect engineering for enhanced ultrasonic piezocatalytic therapy of bacteria-infected bone defects. Chem Eng J 2022;435:134624.
[23] Wang T, Ouyang H, Luo Y, et al. Rehabilitation exercise-driven symbiotic electrical stimulation system accelerating bone regeneration. Sci Adv 2024;10: eadi6799.
[24] Ge M, Ge K, Gao F, et al. Biomimetic mineralized strontium-doped hydroxyapatite on porous poly(L-lactic acid) scaffolds for bone defect repair. Int J Nanomed 2018;13:1707–21.
[25] Jin SS, He DQ, Luo D, et al. A biomimetic hierarchical nanointerface orchestrates macrophage polarization and mesenchymal stem cell recruitment to promote endogenous bone regeneration. ACS Nano 2019;13:6581–95.
[26] Groen N, Yuan HP, Hebels D, et al. Linking the transcriptional landscape of bone induction to biomaterial design parameters. Adv Mater 2017;29:1603259.
[27] Zhang YZ, Xu LL, Liu Z, et al. Self-powered pulsed direct current stimulation system for enhancing osteogenesis in MC3T3-E1. Nano Energy 2021;85:106009.
[28] Pobloth A-M, Checa S, Razi H, et al. Mechanobiologically optimized 3D titanium-mesh scaffolds enhance bone regeneration in critical segmental defects in sheep. Sci Transl Med 2018;10:eaam8828.
[29] Chen SX, Wang HJ, Mainardi VL, et al. Biomaterials with structural hierarchy and controlled 3D nanotopography guide endogenous bone regeneration. Sci adv 2021;7:31.
[30] Jakus AE, Rutz AL, Jordan SW, et al. Hyperelastic "bone": A highly versatile, growth factor-free, osteoregenerative, scalable, and surgically friendly biomaterial. Sci Transl Med 2016;8:358.
[31] Kong Y, Duan JZ, Liu F, et al. Regulation of stem cell fate using nanostructure-mediated physical signals. Chem Soc Rev 2021;50:12828–72.
[32] Liu Y, Dzidotor G, Le TT, et al. Exercise-induced piezoelectric stimulation for cartilage regeneration in rabbits. Sci Transl Med 2022;14:eabi7282.
[33] Tai YY, Yang S, Yu S, et al. Modulation of piezoelectric properties in electrospun PLLA nanofibers for application-specific self-powered stem cell culture platforms. Nano Energy 2021;89:106444.
[34] Lee H, Dellatore SM, Miller WM, et al. Mussel-inspired surface chemistry for multifunctional coatings. Science 2007;318:426–30.
[35] Xia GB, Wang GB, Yang HY, et al. Piezoelectric charge induced hydrophilic poly (L-lactic acid) nanofiber for electro-topographical stimulation enabling stem cell differentiation and expansion. Nano Energy 2022;102:107690.
[36] Bez M, Sheyn D, Tawackoli W, et al. In situ bone tissue engineering via ultrasound-mediated gene delivery to endogenous progenitor cells in mini-pigs. Sci Transl Med 2017;9:eaal3128.
[37] Zhang XZ, Jiang W, Xie C, et al. Msx1^{+} stem cells recruited by bioactive tissue engineering graft for bone regeneration. Nat Commun 2022;13:5211.
[38] Jiang FY, Shan YZ, Tian JY, et al. Poly(L-lactic acid) nanofiber-based multilayer film for the electrical stimulation of nerve cells. Adv Mater Interfaces 2023;10:2202474.
[39] Chen CJ, Zhao SL, Pan CF, et al. A method for quantitatively separating the piezoelectric component from the as-received "Piezoelectric" signal. Nat Commun 2022;13:1391.
[40] Watanabe Y, Nakayama T, Nagakubo D, et al. Dopamine selectively induces migration and homing of naive CD8^{+} T cells via dopamine receptor D3. J Immunol 2006;176:848–56.
[41] Wang X, Agrawal V, Dunton CL, et al. Chromatin reprogramming and bone regeneration *in vitro* and *in vivo* via the microtopography-induced constriction of cell nuclei. Nat Biomed Eng 2023;7:1514–29.
[42] Chai YC, Carlier A, Bolander J, et al. Current views on calcium phosphate osteogenicity and the translation into effective bone regeneration strategies. Acta Biomater 2012;8:3876–87.
[43] He YN, Li F, Jiang P, et al. Remote control of the recruitment and capture of endogenous stem cells by ultrasound for *in situ* repair of bone defects. Bioact Mater 2023;21:223–38.
[44] Lu GG, Xu Y, Liu QY, et al. An instantly fixable and self-adaptive scaffold for skull regeneration by autologous stem cell recruitment and angiogenesis. Nat Commun 2022;13:2499.
[45] Tian JJ, Shi R, Liu Z, et al. Self-powered implantable electrical stimulator for osteoblasts' proliferation and differentiation. Nano Energy 2019;59:705–14.
[46] Ripamonti U, Roden LC, Renton LF. Osteoinductive hydroxyapatite-coated titanium implants. Biomaterials 2012;33:3813–23.
[47] Lu MX, Chen HJ, Yuan B, et al. The morphological effect of nanostructured hydroxyapatite coatings on the osteoinduction and osteogenic capacity of porous titanium. Nanoscale 2020;12:24085–99.
[48] Shi Y, He L, Deng Q, et al. Synthesis and applications of silver nanowires for transparent conductive films. Micromachines 2019;10:330.
[49] Cheng L, Chen Z, Cai Z, et al. Bioinspired functional black phosphorus electrospun fibers achieving recruitment and biomineralization for staged bone regeneration. Small 2020;16:2005433.

Xi Cui received her Bachelor's degree from Jilin University in 2019. She is currently pursuing the Ph.D. degree at Beijing Institute of Nanoenergy and Nanosystems, Chinese Academy of Sciences. Her research mainly focuses on piezoelectric bone implant materials.

Lingling Xu received her Bachelor's and Master's degrees from Sichuan University in 2015 and 2018, respectively, and her Ph.D. degree from the University of Chinese Academy of Sciences in 2021. She is now a postdoctoral research fellow at the National Center for Nanoscience and Technology of China. Her research interest includes stimulus-responsive drug delivery systems and biomedical systems.

Dan Luo received his B.Sc. and Ph.D. degrees from Peking University Health Science Center in 2008 and 2013, respectively. He worked at Institute of Chemistry, Chinese Academy of Sciences in 2013, and then transferred to China University of Petroleum-Beijing in 2015. Since 2021, he has joined the Beijing Institute of Nanoenergy and Nanosystems, Chinese Academy of Sciences as a professor. His research focuses on physiotherapy strategies based on self-powered devices.

Chunying Chen received her Bachelor's degree in chemistry and obtained her Ph.D. degree in biomedical engineering from Huazhong University of Science and Technology of China. Her research interest focuses on analysis methods and chemobiological effects of nano-protein coronas, detection methods and mechanisms on *in vivo* behavior of nanomaterials, and nano-adjuvants and delivery systems.

Zhou Li received his Ph.D. degree from Peking University, China, in 2010, and his bachelor's degree from Wuhan University, China, in 2004. He is a professor at the Beijing Institute of Nanoenergy and Nanosystems, and School of Nanoscience and Technology, University of Chinese Academy of Sciences. His research interest focuses on wearable and implantable electronic health monitoring and therapy devices, biosensors, biodegradable electronics, and biomechanical investigations.

Please cite this article as: X. Cui, L. Xu, Y. Shan et al., Piezocatalytically-induced controllable mineralization scaffold with bone-like microenvironment to achieve endogenous bone regeneration, Science Bulletin, https://doi.org/10.1016/j.scib.2024.04.002